Norbornane: An investigation into its valence electronic structure using electron momentum spectroscopy, and density functional and Green's function theories

S. Knippenberg
Department SBG, Limburgs Universitair Centrum, Gebouw D, B-3590 Diepenbeek, Belgium

K. L. Nixon, M. J. Brunger,[a] T. Maddern, L. Campbell, and N. Trout
School of Chemistry, Physics and Earth Sciences, Flinders University, GPO Box 2100, Adelaide SA 5001, Australia

F. Wang
Centre for Molecular Simulation, Swinburne University of Technology, PO Box 218, Hawthorn, Vic 3122, Australia

W. R. Newell
Department of Physics and Astronomy, University College, Gower Street, London, United Kingdom and School of Chemistry, Physics and Earth Sciences, Flinders University, GPO Box 2100, Adelaide SA 5001, Australia

M. S. Deleuze and J.-P. Francois
Department SBG, Limburgs Universitair Centrum, Gebouw D, B-3590 Diepenbeek, Belgium

D. A. Winkler
CSIRO Molecular Science, Private Bag 10, Clayton South MDC, Vic 3169, Australia

(Received 19 May 2004; accepted 3 August 2004)

We report on the results of an exhaustive study of the valence electronic structure of norbornane (C_7H_{12}), up to binding energies of 29 eV. Experimental electron momentum spectroscopy and theoretical Green's function and density functional theory approaches were all utilized in this investigation. A stringent comparison between the electron momentum spectroscopy and theoretical orbital momentum distributions found that, among all the tested models, the combination of the Becke-Perdew functional and a polarized valence basis set of triple-ζ quality provides the best representation of the electron momentum distributions for all of the 20 valence orbitals of norbornane. This experimentally validated quantum chemistry model was then used to extract some chemically important properties of norbornane. When these calculated properties are compared to corresponding results from other independent measurements, generally good agreement is found. Green's function calculations with the aid of the third-order algebraic diagrammatic construction scheme indicate that the orbital picture of ionization breaks down at binding energies larger than 22.5 eV. Despite this complication, they enable insights within 0.2 eV accuracy into the available ultraviolet photoemission and newly presented $(e,2e)$ ionization spectra, except for the band associated with the $1a_2^{-1}$ one-hole state, which is probably subject to rather significant vibronic coupling effects, and a band at ~25 eV characterized by a momentum distribution of ''*s*-type'' symmetry, which Green's function calculations fail to reproduce. We note the vicinity of the vertical double ionization threshold at ~26 eV.
[DOI: 10.1063/1.1799014]

I. INTRODUCTION

In spite of the importance of norbornane (NBA) to chemical and pharmaceutical research,[1,2] the experimental determination of its structure has been problematic. The molecule has an extremely small dipole moment [~0.09 D (Ref. 3)], making structural determination by microwave spectroscopy very difficult. Choplin[3] studied the microwave response of norbornane but was unable to determine its structure because of the weak intensity of rotational transitions, due to the low dipole moment, as well as difficulties in preparing isotopically enriched samples. There have been a number of structural studies by electron diffraction[4] but the norbornane molecule is problematic due to strong correlations between parameters used to determine the similar carbon-carbon bond lengths in the molecule. The use of x-ray crystallography to determine an unambiguous structure was complicated by the fact that norbornane, like many globular molecules, is orientationally disordered at ambient temperatures, transforming from cubic to hexagonal at 306 K. Single crystals of norbornane have not been available, and Fitch and Jobic[5] only recently solved the structure by powder x-ray diffraction meth-

[a]Author to whom correspondence should be addressed. Electronic mail: Michael.Brunger@flinders.edu.au

ods using a synchrotron radiation source. However this structure was for solid norbornane, and structures from x-ray diffraction are subject to substantial deformation because of crystal lattice interactions. Consequently, a precise gas phase structure of norbornane has not been determined experimentally and computational approaches have been valuable in interpreting the available experimental data in a consensus fashion. van Alsenoy and co-workers[6] employed *ab initio* Hartree–Fock (HF) calculations to assist in the interpretation of the microwave structure model,[6] and Allinger's group[7] used molecular mechanics methods to analyze the x-ray diffraction and electron diffraction data to give a consistent structure for norbornane.

An experimental calibration of the model employed (i.e., theoretical approach and basis set) using electron momentum spectroscopy (EMS) provides a way to select a wave function which is reliable enough for accurately predicting the molecular structure of norbornane, as well as calculating other important molecular properties such as the dipole moment, bond orders, charge distributions, nuclear magnetic resonance (NMR), and vibrational spectra. Previous studies[7,8] have used a variety of molecular mechanics and molecular orbital approaches to determine structural and electronic properties of norbornane. Here we use the unique orbital imaging capability[9,10] of EMS to determine which of the employed density functional theory (DFT) exchange correlation functionals and basis sets best describes the experimental momentum distributions. This optimum basis and exchange correlation functional is then used to derive the structure and molecular properties of norbornane. These data are next compared with independent experimentally determined values, and those from other molecular orbital (MO) calculations, to determine how well the optimum model was able to reproduce norbornane's molecular properties.

While conducting our study, it became quite clear that existing investigations into the outer and inner valence electronic structure of norbornane are rather scarce. Previous photoelectron spectroscopy (PES) studies include the He(I) measurements from Bischof *et al.*[11] and Getzlaff and Schönhense[12] and the He(II) measurement from Bieri *et al.*[13] Theoretical interpretation of these spectra has been even more limited with only the modified intermediate neglect of differential overlap, version 2 (MINDO/2), result from Bodor *et al.*[14] currently being available in the literature. Hence the present HF, DFT, and one-particle Green's function (1p-GF) calculations significantly expand the available theoretical knowledge of the electronic structure of norbornane. In addition, we believe that the present EMS measurements are the first to be made on this molecule, thus further expanding our understanding of its electronic structure through our original momentum space images of its MO's.

Finally, we note that norbornane is the second molecule in the chemically similar series norbornadiene(I),[15,16] norbornene(II), and norbornane(III), which we have studied using EMS, HF, and DFT techniques. In going from I to III the C=C double bonds in these highly strained bicyclic hydrocarbons are progressively saturated. It is our thesis that by unraveling the electronic structure of norbornane using EMS in conjunction with DFT calculations and the 1p-GF theory of ionization, we may probe the influence of substantial cyclic strains on chemical bonds. In this respect we note our preliminary study[17] on all three molecules I–III, a paper which arose from an invited presentation at the Sagamore 14th meeting.

In the following section of this paper we briefly discuss our EMS measurements, including our ionization spectra. Details of our HF, DFT, and 1p-GF calculations, and some of the electronic structure information we can extract from them are presented in Secs. III and IV, while in Sec. V we compare and discuss the experimental and theoretical momentum distributions associated to all bands in the EMS ionization spectra. In Sec. VI the molecular property information derived from our optimum basis set and exchange correlation functional is detailed, while in Sec. VII some of the conclusions drawn from the current study are presented.

II. EXPERIMENTAL DETAILS AND PRELIMINARY ANALYSIS

A sample of high-purity norbornane was synthesized ''in house'' using commercially purchased (Aldrich Chemical Company) norbornene in the following manner. To a thick-walled flask we added norbornene (5 g, 52 mmol), AR methanol (100 ml), and a spatula amount of 10% Pd on carbon. The resulting mixture was hydrogenated under 40 psi of H_2 for 12 h with rocking. There was an instantaneous uptake of H_2. More H_2 was introduced and left overnight. Water was added and then extracted with $CFCl_3$ (2×20 ml). The bottom organic layer was collected and allowed to evaporate at room temperature. The crude norbornane (~1 g) was pure according to gas chromatographic (GC) and ^{13}C and ^{1}H NMR analysis agreed with previously reported data.[18] This material was then distilled into a U tube immersed in liquid nitrogen and under vacuum and then transferred into the reaction vessel. The reaction vessel was in turn connected to the gas handling system of the EMS spectrometer. In addition, it was degassed *in situ* by repeated freeze-pump-thaw cycles before being introduced into the interaction region. Comparing our $\phi=0°+10°$ ionization spectrum with the PES result of Bischof *et al.*[11] shows that the level of qualitative agreement between them is very good. This gives further evidence for the purity of our NBA sample, an important consideration given the high sensitivity of EMS to the presence of any impurities.

All the 20 occupied MO's of the complete valence region of NBA, namely the $3a_2$, $5b_2$, $7a_1$, $5b_1$, $6a_1$, $4b_2$, $2a_2$, $4b_1$, $3b_2$, $3b_1$, $5a_1$, $2b_1$, $4a_1$, $2b_2$, $3a_1$, $1a_2$, $2a_1$, $1b_2$, $1b_1$, and $1a_1$ MO's, were then investigated in several experimental runs using the Flinders symmetric noncoplanar EMS spectrometer.[9] Details of this coincidence spectrometer and the method of taking the data can be found in the work by Brunger and Adcock,[10] and Weigold and McCarthy,[9] and so we do not repeat them again here.

The high-purity NBA is admitted into the target chamber through a capillary tube, the flow rate being controlled by a variable leak value. Possible clustering, due to supersonic expansion, was avoided by maintaining a low NBA driving pressure throughout data collection. The collision region is differentially pumped by a 700 $l\,s^{-1}$ diffusion pump. Aper-

tures and slits are cut in the collision chamber for the incident electron beam and the scattered and ejected electrons. The differentially pumped collision region makes it possible to increase the target gas density by a factor ~3 while keeping the background pressure below 10^{-5} Torr. This was important as it enabled us to maintain workable coincidence count rates, even with the smaller electron beam current output from the $(e,2e)$ monochromator (typically 30 μA in this work) compared to that of a normal electron gun.[19] The coincident energy resolution of the present measurements was ~0.55 eV full width at half maximum (FWHM) as determined from measurements of the binding-energy (ϵ_f) spectrum of helium. Note that the profile of the helium spectrum was found to be well represented by a Gaussian function. However, due to the natural and vibrational linewidths (sometimes also known as the Franck–Condon widths) of the various electronic transitions and a quite strong dispersion of the ionization intensity into many-electron processes at the bottom of the carbon-2s region, the fitted resolutions of the spectral peaks for NBA varied from ~0.88 to 2.31 eV (FWHM). It is precisely this limitation which forces us to combine our measured highest occupied molecular orbital (HOMO) and next highest occupied molecular orbital (NHOMO) ($3a_2$ and $5b_2$) momentum distributions (MD's), $5b_1$ and $6a_1$ orbital MD's, $4b_2$, $2a_2$, and $4b_1$ orbital MD's, $3b_2$ and $3b_1$ orbital MD's, $5a_1$ and $2b_1$ orbital MD's, and $2a_1$, $1b_2$, and $1b_1$ orbital MD's, respectively. While there is no doubt one loses some physical information in combining these MD's, to not do so would have raised serious question as to the uniqueness of the MD's derived in the fits to our binding energy spectra (see below). The angular resolution, which determines the momentum resolution [see Eq. (1)] was typically 1.2° (FWHM), as determined from the electron optics and apertures and from a consideration of the argon 3p angular correlation.

In the present study, noncoplanar symmetric kinematics were employed; that is, the outgoing electron energies E_A and E_B were equal (=750 eV) and the scattered (A) and ejected (B) electrons made equal polar angles, θ=45°, with respect to the direction of the incident electrons. The total energy E ($E=E_0-\epsilon_f=E_A+E_B$) was 1500 eV. The beam energy is E_0. The binding-energy range of interest ($\epsilon_f=7-29$ eV) is stepped through sequentially at each of a chosen set of angles ϕ using a binning mode[19] through the entire set of azimuthal angles (ϕ=0°–30°). Scanning through a range of ϕ is equivalent to sampling different target electron momenta p as[9]

$$p=\left[(2p_A\cos\theta-p_0)^2+4p_A^2\sin^2\theta\sin^2\left(\frac{\phi}{2}\right)\right]^{1/2}. \qquad (1)$$

For zero binding energy (ϵ_f=0 eV), ϕ=0° corresponds to $p=0$ a.u., and for the present binding energies, angular resolution, and kinematics, ϕ=0° corresponds to $p\approx0.03$ a.u. Note that 1 a.u.$\equiv 1a_0^{-1}$, where a_0 is the Bohr radius.

Ionization spectra of norbornane measured at representative angles ϕ in the region 7–29 eV and at $E=1500$ eV are displayed in Fig. 1. The solid curve in each panel represents the envelope of the 13 fitted Gaussians (various dashed curves) whose positions below $\epsilon_f\sim23$ eV are taken from the available PES data.[11–13] A summary of the available orbital binding energies from PES data, the present EMS binding energies and our tentative orbital assignments are given in Table I. The fact that we use only 13 Gaussians to analyze spectra containing 20 valence MO's simply reflects our earlier point that our energy resolution was insufficient to uniquely deconvolve all the orbitals, so that some were combined (summed). Notwithstanding this it is clear from Fig. 1 that the fits to the measured binding-energy spectra are excellent. The least-squares-fit deconvolution technique used in the analysis of these spectra is based on the work of Bevington and Robinson,[20] to whom readers are referred for more detail. Above $\epsilon_f\sim23$ eV there are no PES data available to guide us in our fitting of the binding-energy spectra. Under these circumstances the positions and widths of the Gaussian peaks and the number of Gaussians used in the spectral deconvolution were simply determined by their utility in best fitting the observed data for all ϕ. The fact that the inner valence $2a_1$, $1b_2$, $1b_1$, and $1a_1$ orbitals need three very broad Gaussians (peaks 11–13) to incorporate the measured coincidence intensity into the fit, is undoubtedly indicative of a severe dispersion of ionization intensity over many satellite states, an observation which led us to undertake thorough 1p-GF calculations of the valence one-electron and shake-up ionization spectrum of norbornane (see Sec. IV).

The EMS ionization spectra of Fig. 1 clearly reflect the respective symmetries[9] of the valence orbitals of norbornane. For instance, the unresolved HOMO and NHOMO (peak 1) show significantly more intensity at ϕ=10° compared to that at ϕ=0°. This is consistent with the ''p-type'' symmetry of these orbitals. On the other hand the $4a_1$ orbital (peak 7) has a much greater intensity at ϕ=0° compared to that found at ϕ=10°, an angular dependence which corroborates its ''s-type'' symmetry. On the basis of the symmetry indicated by the EMS binding-energy spectra and the results of our calculations in Table II (see Secs. III and IV for more details) tentative orbital assignments were made and are given in Table I. In general these orbital assignments are consistent with those found from our 1p-GF calculations, with the exception of band 12 in the inner valence region. The angular dependence of the EMS cross sections indicates that bands 12 and 13 have similar s-type MD's so that both bands at first glance could be ascribed to originating from the $1a_1$ orbital. Our 1p-GF calculations support the notion that band 13 relates essentially to satellites originating from ionization of the $1a_1$ orbital. In addition, the EMS and 1p-GF interpretations of band 11 are largely consistent in assigning that flux as mainly being due to a set of lines related to ionization of the $2a_1$, $1b_2$, and $1b_1$ orbitals. Band 12, however, appears to be a far more complicated issue than was originally anticipated (see Sec. IV).

III. THEORETICAL ANALYSIS OF EMS CROSS SECTIONS

The plane wave impulse approximation[21] (PWIA) is used to analyze the measured cross sections for high-momentum transfer $(e,2e)$ collisions. Using the Born–Oppenheimer approximation for the target and ion wave

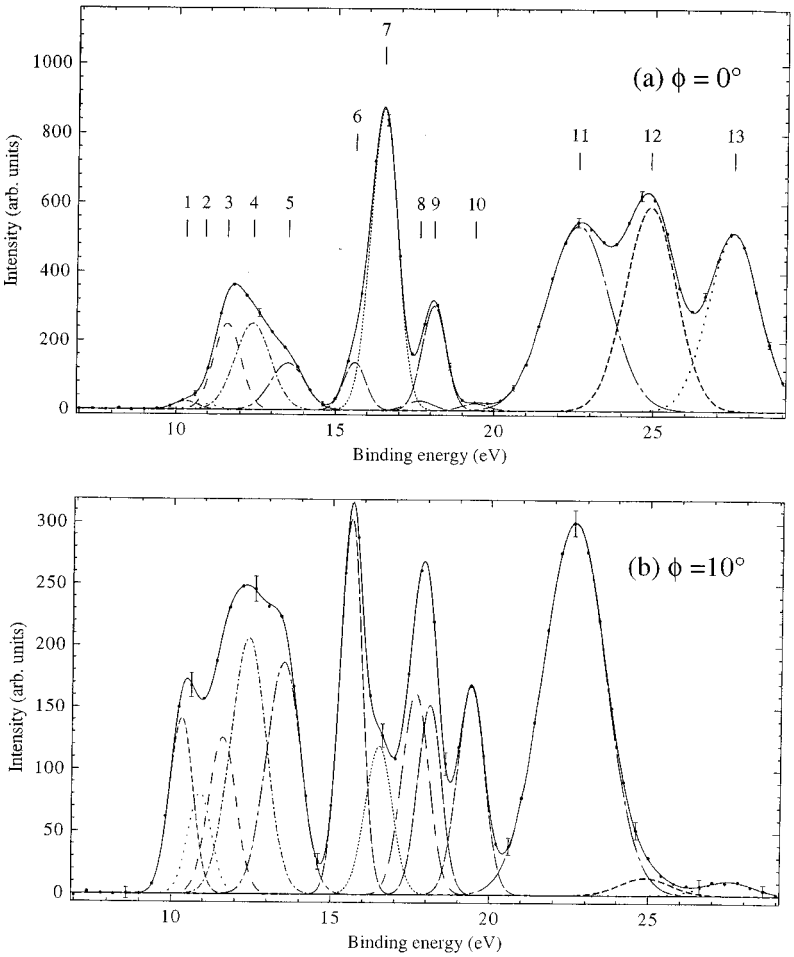

FIG. 1. Typical binding-energy spectra from our 1500 eV noncoplanar symmetric EMS investigation into norbornane. The curves show the fits to the spectra at (a) $\phi=0°$ ($p\approx0.03$ a.u.) and (b) $\phi=10°$ ($p\approx0.92$ a.u.) using the known energy resolution. The peak positions of the Gaussians used in the fit (see also Table I) are indicated. Note that indicative error bars are shown on this figure.

TABLE I. Norbornane—electronic structure (experimental).

Orbital number	Present Classification	ϵ_f (eV) Experimental PES (Ref. 11)	PES (Ref. 12)	PES (Ref. 13)	Present EMS	Natural width (eV) (Refs. 11–13)
1	$3a_2$	~10.2	~10.3	~10.3	10.3	0.72
2	$5b_2$					
3	$7a_1$	~10.7	~10.9	~10.9	10.9	0.72
4	$5b_1$		~11.6	~11.6	11.6	0.86
5	$6a_1$					
6	$4b_2$	~11.4–12.12				
7	$2a_2$		~12.4	~12.4	12.4	1.20
8	$4b_1$					
9	$3b_2$	~13.4	~13.6	~13.5	13.5	1.14
10	$3b_1$					
11	$5a_1$	~15.5	~15.6	~15.6	15.6	0.64
12	$2b_1$					
13	$4a_1$	~16.4	~16.5	~16.5	16.5	0.86
14	$2b_2$	~17.5	~17.5–17.8	~17.65	17.65	0.86
15	$3a_1$	⋯	~18.1	~18.1	18.1	0.72
16	$1a_2$	⋯	~19.4	~19.4	19.4	0.86
17	$2a_1$	⋯	⋯			
18	$1b_2$	⋯	⋯	~22.62	~22.6	2.25
19	$1b_1$	⋯	⋯			
20	$1a_1$ [a]	⋯	⋯	⋯	24.9	1.80
					27.5	1.80

[a]This assignment is controversial. See text.

functions, the EMS differential cross section σ, for randomly oriented molecules and unresolved rotational and vibrational states, is given[9] by

$$\sigma = K \int d\mathbf{\Omega} |\langle \mathbf{p}\Psi_f^{N-1} | \Psi_i^N \rangle|^2, \tag{2}$$

where K is a kinematical factor which is essentially constant in the present experimental arrangement. Ψ_f^{N-1} and Ψ_i^N are the electronic many-body wave functions for the final $[(N-1)$ electron] ion and target [N-electron] ground states, and $\mathbf{p}$ is a plane wave representing the ionized electron. The $\int d\mathbf{\Omega}$ denotes the integral required for averaging the computed $(e,2e)$ cross sections over all gas phase molecular orientations (spherical averaging). The average over the initial vibrational state is well approximated by evaluating orbitals at the equilibrium geometry of the molecule. Final rotational and vibrational states are eliminated by closure.[9]

The momentum space target-ion overlap $\langle \mathbf{p}\Psi_f^{N-1} | \Psi_i^N \rangle$ can be evaluated using configuration interaction descriptions of the many-body wave functions,[22] but usually the weak coupling approximation[19] is made. Here the target-ion overlap is replaced by the relevant orbital of, typically, the Hartree–Fock or Kohn–Sham[23] ground state Φ_0, multiplied by a spectroscopic amplitude. With these approximations Eq. (2) reduces to

$$\sigma = K S_j^{(f)} \int d\mathbf{\Omega} |\phi_j(\vec{p})|^2, \tag{3}$$

where $\phi_j(\vec{p})$ is the momentum space orbital. Note that the relaxation of the final state has been neglected in this approximation. Further, note that the basis of the orbital imaging capability of EMS is immediately apparent from Eq. (3). The spectroscopic factor $S_j^{(f)}$ is the square of the spectroscopic amplitude for orbital j and ion state f. It satisfies the sum rule

$$\sum_j S_j^{(f)} = 1. \tag{4}$$

Hence $S_j^{(f)}$ may be considered as the probability of finding the one-hole configuration in the many-body wave function of the ion.

The Kohn-Sham equation[23] of DFT may be considered as an approximate quasiparticle equation, with the potential operator approximated by the exchange-correlation potential.[22] Often this is done using the local spin density (LSD) approximation, although in this study we concentrate on approximating the exchange-correlation (XC) functional with functionals that depend on the electron density and its gradients[24–27] [i.e., the generalized gradient approximation (GGA)]. Specifically, here we employed two different approximations to the XC energy functional due to Becke and Perdew[24–26] (BP) and Becke, Lee, Yang, and Parr (BLYP).[24,25,27] To compute the coordinate space Kohn–Sham orbitals ψ_j, we employed DGAUSS, a program package originally developed at CRAY Research by Andzelm and co-workers.[28,29] It has been known for a number of years[30] that HF theory provides momentum distributions of lower quality than DFT, therefore we do not assess HF momentum distributions again here. DGAUSS is itself a part of UniChem.[30] The molecular structure of norbornane has been optimized through energy minimization with various gradient-corrected functionals and basis sets, employing the UniChem user interface. Note that a geometry optimization was performed in DGAUSS with each basis set used. The electronic structural calculations using restricted Hartree–Fock (RHF) and second-order Møller–Plesset (MP2) approaches along with a polarized valence basis set of triple-ζ (TZVP) quality are based on GAMESS.[31] A subset of our calculated orbital energies from both our DFT RHF calculations is given in Table II. Clearly, none of these results give particularly good agreement with the corresponding experimental values of Table I. Despite Koopmans' theorem, all HF orbital energies overestimate the measured ionization energies by $\sim$1 to $\sim$3 eV, which indicates that these energies are substantially influenced by electron-correlation effects, and, more importantly, electron relaxation effects. On the other hand, the BLYP- and BP-DFT orbital energies all underestimate the respective experimental binding energies by $\sim$3.5–4.7 eV. Such a result was, however, not entirely unexpected. It is known (Ref. 32 and references therein) that XC functionals, whether at LSD or GGA levels, fail to give the correct dispersion interaction in the large r region. This error in the asymptotic limit of the XC functionals leads to ionization energies that underestimate those determined by experiment by as much as 5 eV.

TABLE II. Norbornane–electronic structure (theory).

Orbital number	Present Classification	ϵ_f (eV) Basis sets: Present HF/TZVP	Present HF/cc-pVDZ	Present DFT BP/TZVP
1	$3a_2$	11.332	11.328	6.88
2	$5b_2$	11.666	11.641	7.24
3	$7a_1$	12.033	12.006	7.54
4	$5b_1$	12.585	12.531	7.90
5	$6a_1$	12.659	12.607	7.98
6	$4b_2$	13.140	13.108	8.19
7	$2a_2$	13.439	13.384	8.41
8	$4b_1$	13.695	13.634	8.65
9	$3b_2$	14.767	14.734	9.41
10	$3b_1$	14.887	14.831	9.46
11	$5a_1$	17.079	16.999	11.16
12	$2b_1$	17.332	17.232	11.43
13	$4a_1$	18.474	18.360	12.26
14	$2b_2$	19.793	19.772	12.82
15	$3a_1$	20.547	20.500	13.42
16	$1a_2$	22.372	22.328	14.64
17	$2a_1$	25.576	25.542	16.94
18	$1b_2$	26.593	26.570	17.68
19	$1b_1$	27.135	27.067	18.10
20	$1a_1$	31.606	31.532	21.48

Information of the molecular structure and the molecular orbital wave functions for the ground electronic state of NBA, obtained from the DGAUSS DFT calculations, were next treated as input to the Flinders-developed program AMOLD,[19] which computes the momentum space spherically averaged molecular-structure factor[21] and the $(e,2e)$ cross section or MD [see Eq. (3)]. Note that all the theoretical MD's we report in this paper have had the experimental an-

gular resolution folded in using the method of Frost and Weigold.[33]

The comparisons of calculated MD's with experiment (see Sec. V) may be viewed as an exceptionally detailed test of the quality of the XC energy and basis set. From our previous experience,[34,35] the GGA-DFT methods using the BP and BLYP XC functionals give best agreement with the experimental MD's, compared to the LSD method. As a result, GGA-BP and GGA-BLYP are used in combination with three basis sets to examine the behavior of the XC functionals and basis sets. These basis sets are denoted by the acronyms DZVP, DZVP2, and TZVP. The notations DZ and TZ denote basis sets of double- or triple-ζ quality. *V* denotes a calculation in which such a basis is used only for the valence orbitals and a minimal basis is used for the less chemically reactive core orbitals. The inclusion of long-range polarization functions is denoted by *P*. We note, in particular, that the basis sets of DGAUSS were specially designed for DFT calculations.[28,36] The TZVP basis set has a contraction scheme [7111/411/1] for carbon and [3111/1] for hydrogen. The auxiliary basis set corresponding to the TZVP basis is called $A1$,[37] in which the *s*-, *p*-, and *d*-orbital exponents were determined separately from an optimization that reproduces, as accurately as possible, the energy from an atomic DFT calculation. The contraction schemes of the $A1$ basis sets for H are [4/1] and for C [8/4/4].

The DFT DGAUSS calculations were performed on a Silicon Graphics 02 (R5200) workstation as the UniChem client and a CRAY *J*90*se*/82048 computer as the DFT computational engine. Further restricted Hartree–Fock (RHF) and MP2 calculations using the TZVP basis set and a GAMESS 02 suite of programs,[31] were carried out on the Compaq Alpha Server SC cluster at the Australian Partnership for Advanced Computing National Facilities.

In light of the marginal agreement between the DFT and experimental ionization energies, which we described earlier, further calculations employing more sophisticated Green's function techniques were undertaken. These calculations are all based on geometries that have been optimized using density functional theory by means of the GAMESS 02 program[31] employing the TZVP basis set and the nonlocal hybrid Becke three-parameter Lee–Yang–Parr functional (B3LYP).[27,38]

IV. THEORETICAL ANALYSIS OF VALENCE IONIZATION SPECTRA

Vertical ionization spectra have been computed using one-particle Green's function (1p-GF) theory at the level of the third-order algebraic diagrammatic construction [ADC(3)] scheme,[39–42] in conjunction with Dunnings' correlation consistent polarized valence basis set of double-ζ quality [cc-pVDZ (Ref. 43)], and with the original code interfaced to the GAMESS 92 package.[31] With the 1p-GF/ADC(3) approach, the primary one-hole $(1h)$ and the shake-up two-hole-one-particle $(2h\text{-}1p)$ ionization energies are recovered through third and first order in correlation, respectively. Constant self-energy diagrams have been computed through fourth order in correlation, using charge-consistent[44] one-electron densities. A threshold on pole strengths of 0.005 has been retained for solving the ADC(3) secular equation, using a Block-Davidson diagonalization procedure[45] in the final diagonalization step. The assumption of frozen core electrons has been used throughout and symmetry has been exploited to the extent of the C_{2v} point group. Our results from these calculations are presented in Table III. For comparison purposes, more specifically to evaluate the sensitivity of the computed ionization energies to the quality of the basis set, a few results obtained from outer-valence Green's function [OVGF (Refs. 46, 47)] calculations, performed with the GAUSSIAN 98 package,[48] are also presented in Table III. For these benchmark computations of one-electron ionization energies, specifically, we will consider basis sets such as Dunning's correlation consistent polarized valence basis set of triple-ζ quality [cc-pVTZ (Ref. 43)], and the cc-pVDZ basis augmented by a set of diffuse $\{s,p\}$ functions on hydrogens, and a set of diffuse $\{s,p,d\}$ functions on carbons [aug-cc-pVDZ (Refs. 43, 49)]. With the cc-pVDZ, aug-cc-pVDZ and cc-pVTZ basis sets, 158, 269, and 378 basis functions in total are incorporated in the OVGF computations on norbornane, respectively.

Because of the complexity of the outermost valence bands, encompassing the contributions of many and strongly overlapping ionization lines, it is preferable to resort to theoretical simulations for analyzing the available PES measurements. As a guide to the eye, the identified solutions of the secular ADC(3)/cc-pVDZ eigenvalue problem are therefore displayed as a spike spectrum and in the form of a convoluted density of states, along with the ultraviolet photoionization spectra by Getzlaff and Schönhense[12] and Bieri *et al.*[13] (see Fig. 2 and Table III). The convolution has been performed using as a spread function a combination of a Gaussian and a Lorentzian with equal weight, a FWHM parameter of 0.6 eV, and by simply scaling the line intensities according to the computed ADC(3) pole (spectroscopic) strengths. Despite the neglect of cross section effects, the shape, position and the relative intensities of bands in the He(I) and He(II) spectra are overall very finely reproduced in the simulation. In particular, in line with the convoluted spectrum, three substructures are seen with the outermost He(II) ionization band, namely, a shoulder at ~10.9 eV, and two maxima at ~11.7 and ~12.1 eV.

There are several points we would like to highlight from the results in Table III: First, the current Green's function results for ϵ_f of each respective orbital are in satisfactory agreement with those correspondingly found in the previous PES work[11–13] (see Fig. 2) and present EMS study (see Table I), particularly for the outer valence orbitals. Second, our ADC(3) results predict that the ionization intensity resulting from the inner valence $2a_1$, $1b_2$, $1b_1$, and $1a_1$ orbitals is severely split due to final state electron correlation effects. For these orbitals, the fractions of intensity recovered under the form of lines with a spectroscopic strength larger than 0.005 amount to 0.765, 0.697, 0.725, and 0.481, respectively. This observation is entirely consistent with previous one-particle Green's function[50–53] or MR-SDCI (Ref. 54) studies of the ionization spectra of saturated hydrocarbons larger than ethane. As has been noted earlier,[50,51] the dispersion of ionization intensity over many shake-up lines at energies larger than 22 eV correlates well with significant band broad-

TABLE III. Norbornane—electronic structure (theory). Binding energies are given in eV, along with the OVGF and ADC(3) spectroscopic factors in parentheses. Results obtained using (I) B3-YP/TZVP, (II) B3LYP/cc-pVTZ, and MP2/aug-cc-pVDZ geometries.

			ϵ_f (eV) Basis sets					
Symbol	Orbital number	Present classification	Present ADC(3)/ cc-pVDZ (I)	Present OVGF/ cc-pVDZ (I)	Present OVGF/ aug-cc-pVDZ (I)	Present OVGF/ cc-pVTZ (I)	Present OVGF/ cc-pVTZ (II)	Present OVGF/ cc-pVTZ (III)
u	1	$3a_2$	10.513 (0.91)	10.390 (0.91)	10.467 (0.91)	10.443 (0.91)	10.392 (0.91)	10.359 (0.91)
t	2	$5b_2$	10.863 (0.91)	10.746 (0.91)	10.830 (0.91)	10.793 (0.91)	10.758 (0.91)	10.734 (0.91)
s	3	$7a_1$	11.189 (0.91)	11.063 (0.91)	11.154 (0.91)	11.121 (0.91)	11.075 (0.91)	11.055 (0.91)
r	4	$5b_1$	11.657 (0.90)	11.513 (0.91)	11.607 (0.91)	11.555 (0.91)	11.534 (0.91)	11.507 (0.91)
q	5	$6a_1$	11.670 (0.91)	11.529 (0.91)	11.615 (0.91)	11.557 (0.91)	11.554 (0.91)	11.507 (0.91)
p	6	$4b_2$	12.102 (0.91)	11.986 (0.91)	12.072 (0.91)	12.043 (0.91)	11.995 (0.91)	11.975 (0.91)
n	7	$2a_2$	12.445 (0.91)	12.390 (0.91)	12.453 (0.91)	12.452 (0.91)	12.406 (0.91)	12.353 (0.91)
m	8	$4b_1$	12.645 (0.90)	12.545 (0.91)	12.629 (0.91)	12.592 (0.91)	12.569 (0.91)	12.518 (0.91)
l	9	$3b_2$	13.657 (0.90)	13.589 (0.91)	13.670 (0.91)	13.650 (0.91)	13.605 (0.91)	13.557 (0.91)
k	10	$3b_1$	13.736 (0.90)	13.687 (0.91)	13.762 (0.91)	13.755 (0.91)	13.706 (0.91)	13.635 (0.91)
j	11	$5a_1$	15.757 (0.89)	15.587 (0.91)	15.624 (0.90)	15.650 (0.90)	15.619 (0.91)	15.552 (0.91)
i	12	$2b_1$	15.948 (0.89)	15.734 (0.90)	15.771 (0.90)	15.784 (0.90)	15.772 (0.90)	15.685 (0.91)
h	13	$4a_1$	16.897 (0.88)	16.698 (0.90)	16.740 (0.89)	16.741 (0.89)	16.746 (0.90)	16.649 (0.90)
g	14	$2b_2$	17.866 (0.86)	17.817 (0.89)	17.843 (0.89)	17.872 (0.89)	17.831 (0.89)	17.741 (0.89)
f	15	$3a_1$	18.473 (0.86)	18.405 (0.88)	18.435 (0.88)	18.449 (0.88)	18.429 (0.88)	18.335 (0.88)
e	16	$1a_2$	19.926 (0.83)	19.953 (0.87)	19.979 (0.87)	19.988 (0.87)	19.980 (0.88)	19.881 (0.87)
d	17	$2a_1$	21.695 (0.02)[a]	22.560 (0.85)[b]	22.588 (0.85)[b]	22.566 (0.85)	22.595 (0.85)[b]	22.497 (0.85)[b]
			22.088 (0.09)[c]					
			22.389 (0.13)[d]					
			22.484 (0.51)					
			23.573 (0.01)					
			23.961 (0.01)					
c	18	$1b_2$	22.493 (0.01)	23.288 (0.84)[b]	⋯	23.286 (0.84)[b]	23.327 (0.84)[b]	23.256 (0.84)[b]
			22.951 (0.39)					
			22.960 (0.02)					
			23.053 (0.04)					
			23.162 (0.07)					
			23.235 (0.01)					
			23.397 (0.01)					
			23.345 (0.08)					
			23.448 (0.04)					
			23.650 (0.02)					
			23.968 (0.01)					
			24.042 (0.01)					
			24.108 (0.02)					
b	19	$1b_1$	22.327 (0.01)	23.786 (0.84)[b]	⋯	23.782 (0.83)[b]	23.834 (0.84)[b]	23.735 (0.84)[b]
			22.555 (0.01)					
			22.810 (0.01)					
			23.167 (0.02)					
			23.190 (0.02)					
			23.287 (0.04)					
			23.378 (0.08)					
			23.444 (0.05)					
			23.456 (0.01)					
			23.533 (0.01)					
			23.597 (0.17)					
			23.663 (0.24)					
			23.708 (0.01)					
			24.091 (0.01)					
			24.177 (0.01)					
			24.263 (0.01)					
			24.452 (0.01)					
			24.514 (0.01)					
a	20	$1a_1$	25.318 (0.01)	⋯	⋯	⋯	⋯	⋯
			25.410 (0.01)					
			25.676 (0.01)					
			26.104 (0.01)					
			26.350 (0.01)					
			26.411 (0.01)					
			26.445 (0.01)					
			26.459 (0.01)					
			26.493 (0.01)					

TABLE III. (*Continued.*)

Symbol	Orbital number	Present classification	ϵ_f (eV) Basis sets: Present ADC(3)/ cc-pVDZ (I)	Present OVGF/ cc-pVDZ (I)	Present OVGF/ aug-cc-pVDZ (I)	Present OVGF/ cc-pVTZ (I)	Present OVGF/ cc-pVTZ (II)	Present OVGF/ cc-pVTZ (III)
			26.581 (0.01)					
			26.655 (0.01)					
			26.669 (0.01)					
			26.685 (0.01)					
			26.729 (0.02)					
			26.804 (0.03)					
			26.917 (0.02)					
			26.930 (0.03)					
a	20	$1a_1$	27.012 (0.01)	···	···	···	···	···
			27.099 (0.01)					
			27.163 (0.01)					
			27.183 (0.02)					
			27.208 (0.01)					
			27.228 (0.01)					
			27.279 (0.04)					
			27.287 (0.01)					
			27.331 (0.03)					
			27.352 (0.01)					
			27.368 (0.01)					
			27.385 (0.01)					
			27.393 (0.01)					
			27.402 (0.01)					
			27.432 (0.02)					
			27.437 (0.01)					
			27.469 (0.02)					
			27.518 (0.01)					
			27.679 (0.01)					
			27.784 (0.01)					
			27.993 (0.01)					

[a]Dominant electronic configuration: $3a_2^{-2}8a_1^{+1}$ ($\mathrm{HOMO}^{-2}\,\mathrm{LUMO}^{+1}$).
[b]Breakdown of the MO picture of ionization; see J. Chem. Phys. **116**, 7012 (2002).
[c]Dominant electronic configuration: $5b_2^{-2}8a_1^{+1}$ [$(\mathrm{HOMO\text{-}1})^{-2}\,\mathrm{LUMO}^{+1}$].
[d]Dominant electronic configuration: $3a_2^{-1}5b_2^{-1}6b_1^{+1}$.

ening on the experimental side [see the FWHM values reported in Table I for peaks 11–13]. Finally, the present calculations confirm the empirical rule[55] (and references therein) that OVGF pole strengths smaller than 0.85 very consistently foretell a breakdown of the MO picture of ionization at the ADC(3) level. In other words, the quasiparticle approach that has been somewhat unfortunately referred to over the last two decades as the OVGF approach, can also be used for inner-valence states as long as the OVGF spectroscopic strengths remain larger than 0.85. Within that part of the spectrum which can be reliably described by one-hole states, i.e., up to binding energies of 20 eV, the OVGF and ADC(3) ionization energies do not differ by more than ~0.13 eV. For the $2a_1$ orbital the MO picture still holds to some extent, since among the identified satellites one of them emerges at 22.5 eV, in the ADC(3) ionization spectrum, with rather dominant intensity ($S_j^{(f)}=0.51$) and a rather clear $2a_1^{-1}$ one-hole character. At higher binding energies, however, the breakdown of the MO picture intensifies and the OVGF approach can no longer be applied. Note that the impact of diffuse functions on the one-hole ionization energies is very limited (<0.1 eV)—see Table III. Convergence, within ~0.1 eV accuracy, of the OVGF/cc-pVDZ and, by extension, ADC(3)/cc-pVDZ ionization energies (with regards to further improvements of the basis set) is also confirmed by comparison with the OVGF/cc-pVTZ results. Finally, the last two columns of Table III, obtained using geometries optimized at the B3LYP/cc-pVDZ and MP2/aug-cc-pVDZ levels, demonstrate the very limited dependence of the computed ionization spectra on details of the molecular structures. All in all, at the ADC(3)/cc-pVDZ level, we thus expect accuracies of ±0.2 eV on the computed *vertical* one-electron ionization energies. Indeed, an agreement better than 0.2 eV is found upon comparing the theoretical one-electron binding energies reported in Table III with the He(I), He(II), and EMS experimental values of Table I.

Nonetheless, a discrepancy of ~0.6 eV is noticed for the $1a_2^{-1}$ ionization line. Although one can never exclude some calibration problems on the experimental side [the He(I) and He(II) ionization energies reported in Ref. 13 can be in error by approximately ±0.2 eV], this unusually large discrepancy most presumably relates to strong geometry relaxation effects and vibronic interactions in a molecule characterized by pronounced cyclic strains. It can in particular be noticed that the corresponding band in the He(I) and He(II) spectra,[12,13] reproduced in Fig. 2, has a very asymmetric shape, which is

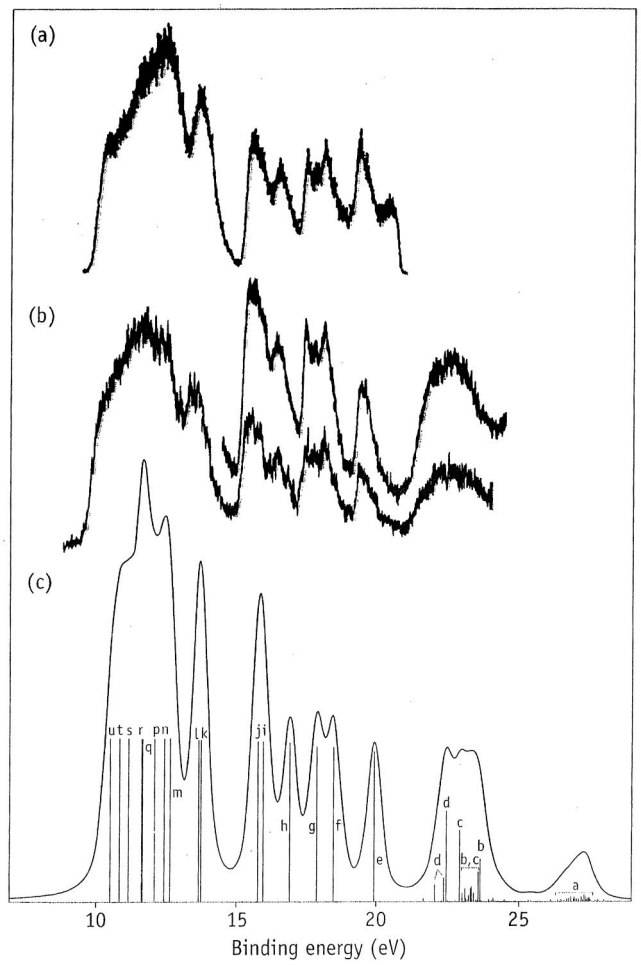

FIG. 2. Comparison between the measured (a) He(I) (Ref. 12), (b) He(II) (Ref. 13), and (c) ADC(3)/cc-pVDZ theoretical ionization spectrum of norbornane.

a quite typical feature for such effects. Further studies of the Franck–Condon vibrational profiles associated to this one-electron ionization line would be necessary for quantitatively clarifying this issue.

The most striking discrepancy between the EMS measurements displayed in Fig. 1 and the ADC(3)/cc-pVDZ spectrum of Fig. 2(c) is the band (12) seen at 24.9 eV in the experimental spectrum, which does not correlate to any set of ionization lines with appreciable enough intensity on the theoretical side. At this point, it is worth recalling that, because of the rather weakly correlated nature of wide band-gap compounds such as saturated hydrocarbons, the expected accuracies of *vertical* one-electron and shake-up ionization energies at the ADC(3)/cc-pVDZ level are around 0.2 (see above) and 0.6 eV, respectively. On the basis of the angular dependence of band 12 (Fig. 1), and of the related MD, which appear to be very similar to that of band 13 (see Sec. V), it would be very tempting to assign both bands to orbital $1a_1$. However, upon examining the ADC(3)/cc-pVDZ simulation of Fig. 2(c) and the corresponding data in Table III, it is immediately apparent that the shake-up lines ascribed to ionization of orbital $1a_1$ concentrate only around 27.5 eV. By analogy with a band–Lanczos study[52] of the valence ionization spectra of *n*-alkanes, the missing fraction (52%) of the $1a_1$ ionization intensity should normally be recovered under the form of an extremely long correlation tail, extending from ~27 eV up to binding energies of 60 eV, and possibly beyond.

Upon performing further MP2/cc-pVDZ calculations of the total energy of norbornane in its neutral and dicationic ground ($^1A_1$) states, including full geometry optimization for both species, it was found that the vertical and adiabatic double ionization potentials of norbornane amount to 25.9 and 23.5 eV, respectively. Further studies, based on two-particle Green's function calculations of doubly ionized states, or highly challenging one-particle Green's function calculations incorporating very diffuse functions, Coulomb and distorted plane waves in the basis set might thus be necessary for identifying with certainty the origin of band 12. Note that, as the $1a_1$ ionization intensity falls clearly much above the double ionization threshold, the shake-up lines which have been identified for that orbital should most correctly be regarded as discrete (bound and excited) cationic states embedded in a continuum of unbound (resonance and shake-off) dicationic states.

Finally, we note that all the MP2, OVGF, and ADC(3) calculations described in Sec. IV were carried out on a DEC-Compaq ES40 workstation at the Limburgs Universitair Centrum in Belgium.

V. COMPARISON BETWEEN EXPERIMENTAL AND THEORETICAL MOMENTUM DISTRIBUTIONS

Deconvolving the ionization spectra measured at each of a chosen set of angles ϕ by means of a least-squares-fit technique[20] allows us to derive the MD's associated to each of the bands identified in Figs. 1(a) and 1(b). Although the measured MD's are not absolute, relative magnitudes for the different transitions are obtained.[19] In the current EMS investigation of the valence states of NBA, the experimental MD's are placed on an absolute scale by summing the experimental flux for each measured ϕ for the first ten outer valence orbitals, and then normalizing this to the corresponding sum for our PWIA-BP/TZVP calculation.

The results from this process for the unresolved HOMO ($3a_2$) and NHOMO ($5b_2$) orbitals are shown in Fig. 3. In this case we find very good agreement between all the calculated PWIA-XC/DFT momentum distributions and our corresponding EMS data taken in two independent runs (runs *A* and *B*). Note that the error bars on all the MD data represent one standard deviation uncertainty. Further, note that the experimental MD data from independent runs *A* and *B* are in very good agreement with one another, a feature that is repeated for all the measured MD's. The results in Fig. 3 strongly suggest that the EMS spectroscopic factors for both the respective $3a_2$ and $5b_2$ orbitals are ~1. This observation is entirely consistent with our calculated ADC(3) and OVGF spectroscopic factors for these orbitals (see Table III). Although not shown, a similar level of agreement between the experimental and theoretical MD's is found for the $7a_1$ orbital. This result implies $S^{\mathrm{EMS}}_{7a_1}(\epsilon_f = 10.9\,\mathrm{eV}) \sim 1$, which is

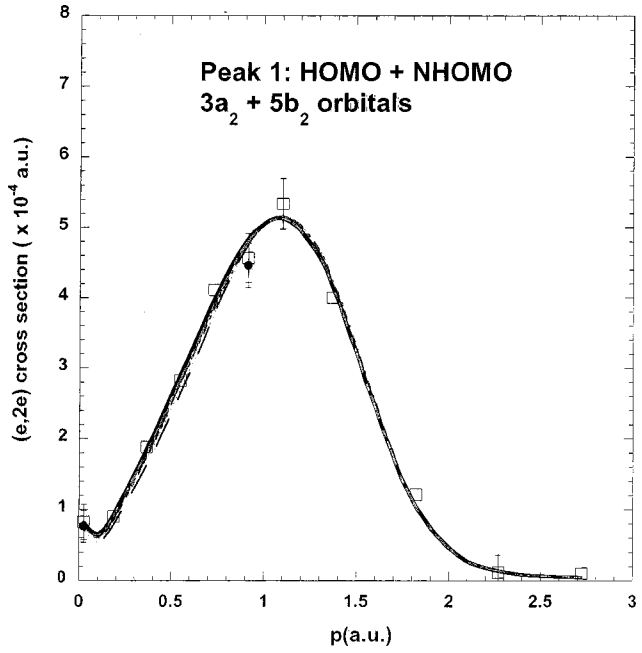

FIG. 3. 1500 eV symmetric noncoplanar MD for the $3a_2+5b_2$ orbitals or norbornane ($\epsilon_f \sim 10.3$ eV). The present data for run *A* (●) and run *B* (□) are compared against the results of our PWIA-DFT calculations: (- - - -) BP/DZVP, (– –) BLYP/DZVP, (· – ·–) BP/DZVP2, (· · · ·) BLYP/DZVP2, (——) BP/TZVP, and (- –) BLYP/TZVP. Acronyms are defined in the text.

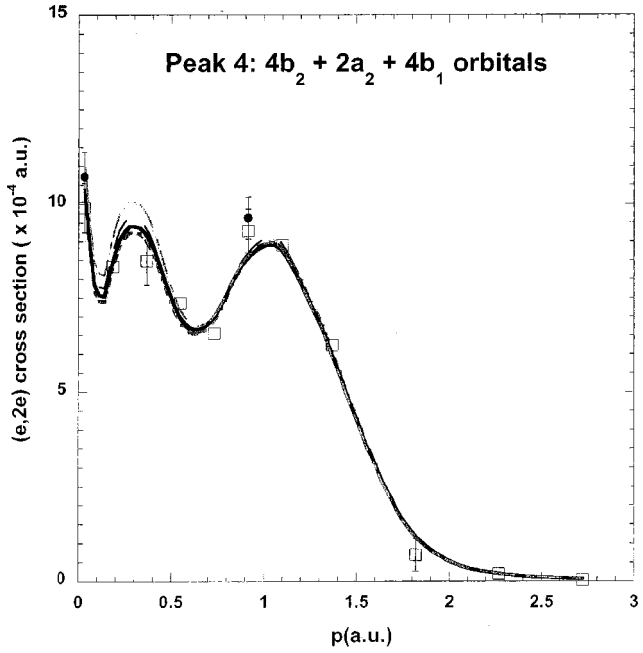

FIG. 5. 1500 eV symmetric noncoplanar MD for the $4b_2+2a_2+4b_1$ orbitals of norbornane ($\epsilon_f \sim 12.4$ eV). The legend is the same as that for Fig. 3.

also in good accord with our calculated ADC(3) and OVGF pole strengths (see again Table III).

In Fig. 4 we show the measured and calculated MD's for the $5b_1+6a_1$ orbitals of norbornane. In this case we find that the momentum distributions calculated at the BLYP/DZVP level within the Plane Wave Impulse Approximation significantly overestimates the magnitude of the experimental cross section for all p. This indicates that the combination

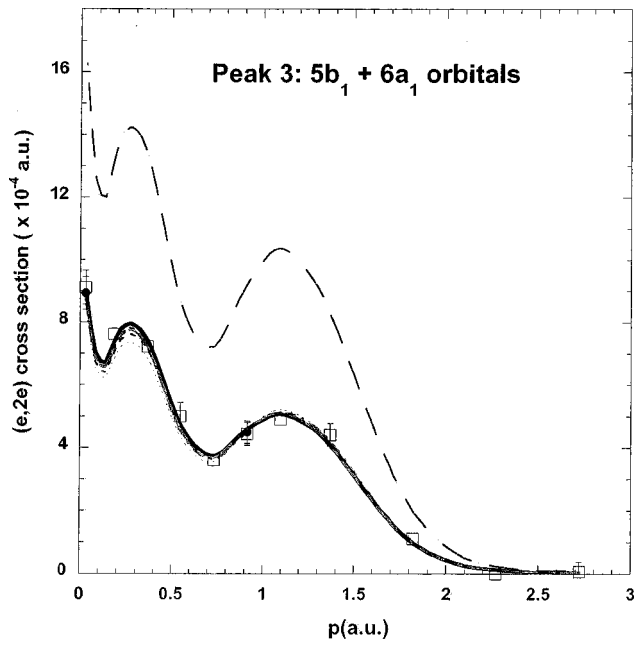

FIG. 4. 1500 eV symmetric noncoplanar MD for the $5b_1+6a_1$ orbitals of norbornane ($\epsilon_f \sim 11.6$ eV). The legend is the same as that for Fig. 3.

of the BLYP exchange correlation functional and DZVP basis set is not providing a very good representation of these orbitals. While it is a less striking effect, Fig. 4 also appears to indicate, for momenta in the region $0.1\ \text{a.u.} \leqslant p \leqslant 0.6\ \text{a.u.}$, that the PWIA-BLYP/DZVP2 MD somewhat underestimates the magnitude of the experimental MD. Nonetheless, the good level of agreement between theory and experiment for the remaining XC/DFT basis set results indicates that the EMS spectroscopic factors of both the $5b_1$ and $6a_1$ orbitals are respectively ~ 1. This finding is consistent with the MO picture of ionization being valid here for these outer-valence orbitals, a result in good agreement with our ADC(3) and OVGF calculations of Table III.

The present MD's for the $4b_2+2a_2+4b_1$ orbitals of norbornane are shown in Fig. 5. In this case there is a very interesting trend for momenta in the range $0.1\ \text{a.u.} \leqslant p \leqslant 0.55\ \text{a.u.}$. Specifically, in this region all the PWIA-BLYP/DFT MD's exhibit a somewhat higher cross section magnitude compared to all the corresponding PWIA-BP/DFT MD's with the experimental cross sections favoring the PWIA-BP/DFT results. This is quite unusual in our experience[10,15,16] as typically we have found that our experimental MD's are more discriminating in terms of the types of basis sets employed, rather than the type of XC functional used. We would characterize the overall level of agreement between our PWIA-BP/DFT momentum distribution results and the experimental momentum distributions as being good, suggesting EMS spectroscopic factors for each of these orbitals lying somewhere in the range 0.9–1.0. Such EMS spectroscopic factors for the $4b_2$, $2a_2$, and $4b_1$ orbitals are found again to be in good agreement with the predictions from our ADC(3) and OVGF calculations, as can be seen in Table III.

The $4a_1$ orbital momentum distributions are illustrated in Fig. 6. In this case we see that all the MD's are strongly

TABLE IV. Experimental and theoretical molecular geometry and dipole moment of norbornane.

Parameter	ED Doms *et al.* (Ref. 6)	x-ray Fitch and Jobic (Ref. 5)	BP/TZVP This work	HF/STO-3G Castro *et al.* (Ref. 58)	HF/3-21G Castro *et al.* (Ref. 58)	HF/4-21G Castro *et al.* (Ref. 58)	HF/4-31G Castro *et al.* (Ref. 58)	MNDO Walklmar *et al.* (Ref. 8)	B3LYP/cc-pVTZ This work	MP2/aug-cc-pVDZ This work
r(C1-C2) (Å)	1.536(15)	1.548	1.549	1.550	1.550	1.551	1.545	1.561	1.543	1.547
r(C1-C7) (Å)	1.546(24)	1.551	1.548	1.544	1.549	1.549	1.544	1.562	1.540	1.546
r(C2-C3) (Å)	1.573(15)	1.578	1.571	1.669	1.571	1.572	1.560	1.558	1.562	1.568
r(C1-H) (Å)	1.113(3)	1.091	1.101	1.087	1.083	1.079	1.084	1.102	1.089	1.101
r(C2-H) (Å)	1.113(3)	1.086, 1.090	1.102	1.087	1.083	1.082	1.084	1.109	1.091	1.102
r(C7-H) (Å)	1.113(3)	1.090	1.102	1.087	1.083	1.082	1.084	1.106	1.091	1.103
∠C1C2C3 (deg)	102.7	106.9	103.11	103.2	103.2	103.1	103.2	103.04	103.08	103.1
∠C1C7C4 (deg)	93.4(1)	93.12	94.52	94.4	94.6	94.6	94.4	93.07	94.42	94.5
∠C2C1C6 (deg)	109.0	110.41	108.82	108.3	107.7	108.0	108.3	109.35	108.47	108.22
∠C2C1C7 (deg)	102.0(1)	99.3	101.35	101.6	101.6	101.6	101.5	101.57	101.54	101.54
∠C7C1H (deg)			116.02	116.4	116.3	116.2	116.3		116.17	116.11
∠HC3H (deg)	107.2	107.64	109.15	112.0, 112.3	110.7, 112.3	110.8, 112.3	110.8, 112.1	106.10	107.33	107.71
∠HC7H′ (deg)	107.2, 110	106.97	109.05	109.4	109.9	109.7	108.9		108.95	109.43
d(C2···C6) (Å)		2.542	2.520						2.504	2.506
μ (D)	0.091(8) MW[a] Choplin (Ref. 3)		0.076						0.089	0.085

[a]MW stands for microwave.

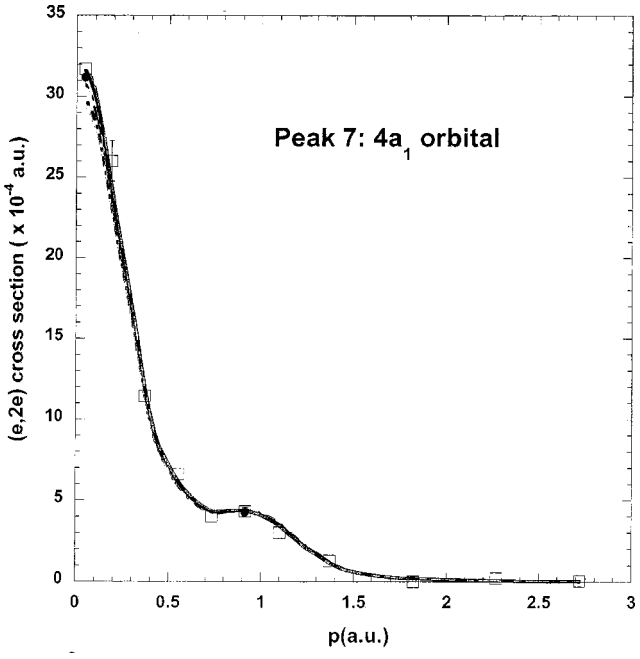

FIG. 6. 1500 eV symmetric noncoplanar MD for the $4a_1$ orbital of norbornane ($\epsilon_f \sim 16.5$ eV). The legend is the same as that for Fig. 3.

peaked (large cross section) as $p \rightarrow 0$ a.u., indicating an s-type symmetry[9] which is probably due to strong C($2s$) contributions. For $p \geqslant 0.2$ a.u. all the theoretical MD's are in good agreement with each other and with the experimental MD results. For $p < 0.2$ a.u., however, only the BP/TZVP, BLYP/TZVP, and, to a lesser extent, the BP/DZVP models are providing a good description of the measurements. When we combine this observation with what we have previously discussed from Figs. 4 and 5, we start to see a trend emerging. Namely, in the one-electron ionization part of the spectrum, the BP/TZVP model gives overall the most accurate description for each of the experimental MD's. Note that this observation also holds for all the MD's we do not specifically plot. Hence, from the results obtained for the one-electron ionization lines, the BP/TZVP wave function appears to be one of the best suited wave functions for studying further structural, vibrational and electronic properties of norbornane—see Sec. VI.

Let us now consider the most challenging part of the ionization spectrum, namely, the inner valence region beyond the shake-up threshold at ~22 eV. In Fig. 7(a) we plot the experimental MD for the sum of peaks 11–13 of Fig. 1, and the corresponding theoretical MD's from the models considered. Here all the theoretical MD's do a fair job in predicting the shape of the experimental result, although they all underestimate the magnitude of the experimental cross section across most of the measured momentum range. This result might reflect a breakdown in the inner valence region for the PWIA description of the reaction mechanism. There certainly exists a large body of evidence that shows that for certain atomic systems[9] the PWIA breaks down for inner valence orbitals. In these cases the $(e,2e)$ ionization process has to be described within a distorted wave framework.[9]

The ADC(3) calculation suggests that peak 11 originates

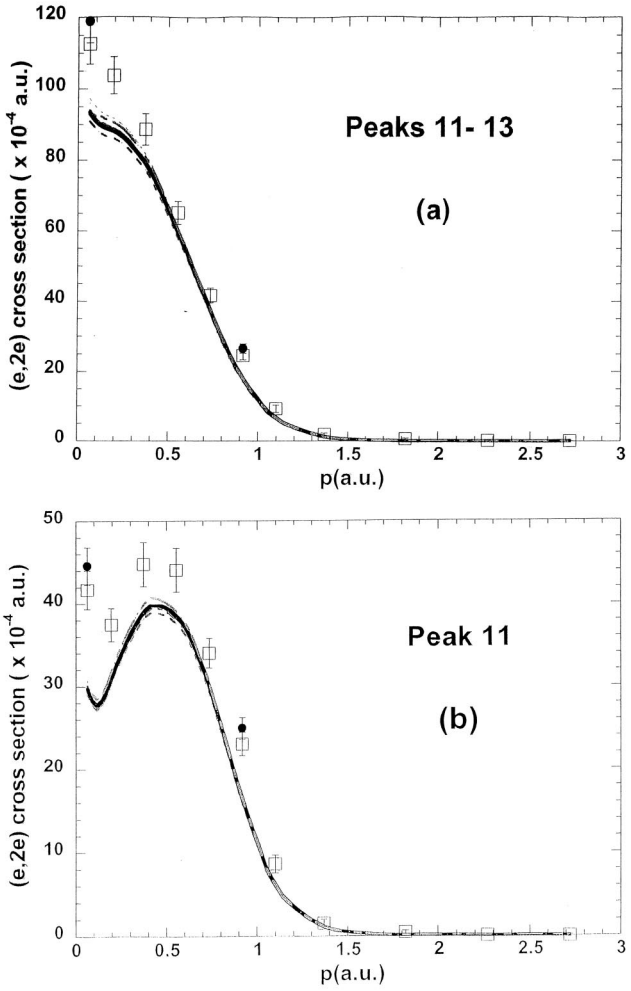

FIG. 7. (a) 1500 eV symmetric noncoplanar MD for peaks 11–13 in the ionization spectrum of norbornane. The legend is the same as that for Fig. 3. (b) 1500 eV symmetric noncoplanar MD for the shake-up band 11 and the $2a_1+1b_1+1b_2$ orbitals of norbornane. The legend is the same as that for Fig. 3.

mainly from the $2a_1$, $1b_2$, and $1b_1$ orbitals and the present EMS experimental MD for this peak supports such a notion. As can be seen from Fig. 7(b), the experimental MD for $2a_1+1b_2+1b_1$ orbitals has very good shape agreement with the corresponding theoretical MD's, although as it might be expected from Fig. 7(a) there is a mismatch in the magnitude of these cross sections. Nonetheless, the present experimental momentum profile exhibits clearly a minimum at $p\sim 0.2$ a.u., in fair agreement with the theoretical predictions for the summed $2a_1+1b_2+1b_1$ orbital set, and thus nicely reflects the fact that band 11 consists of a mixture of ionization lines with *s*-type and *p*-type symmetries.

If we consider the experimental momentum distribution for peak 13, compared to $0.5\times 1a_1$ for PWIA-BP/TZVP (see Fig. 8), then we see that the level of agreement between them is quite good. This is strong evidence that peak 13 largely originates from the innermost valence $1a_1$ orbital, a result which is consistent with our ADC(3) findings. We would like to recall that the missing experimental flux ($\sim$50%) is expected to be found at binding energies beyond the range sampled in the present study. There is evidence in Fig. 1 that

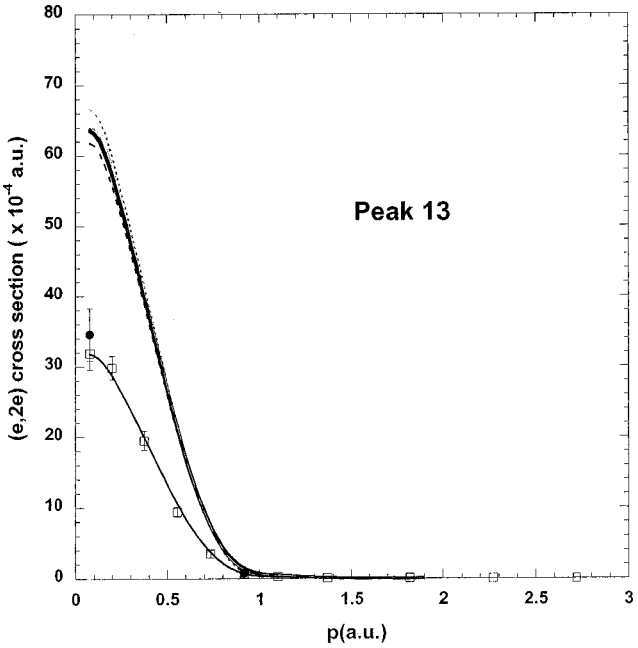

FIG. 8. 1500 eV symmetric noncoplanar MD for the shake-up band 13 and the $1a_1$ orbital of norbornane ($\epsilon_f\sim 27.5$ eV). The legend is the same as that for Fig. 3, except 0.5* BP/TZVP (–) is also shown.

supports the idea that there is additional $1a_1$ flux at $\epsilon_f > 29$ eV. As peak 12 has a similar (although by no means identical) MD to that of peak 13 (see Fig. 9), it is tempting to conclude that it too might originate from the $1a_1$ orbital. However, as noted earlier, our ADC(3) calculation does not support such an assignment. It is possible that peak 12 partly originates from the $2a_1$ orbital with some additional $1b_1$ and $1b_2$ contributions. Such a scenario is allowed by our

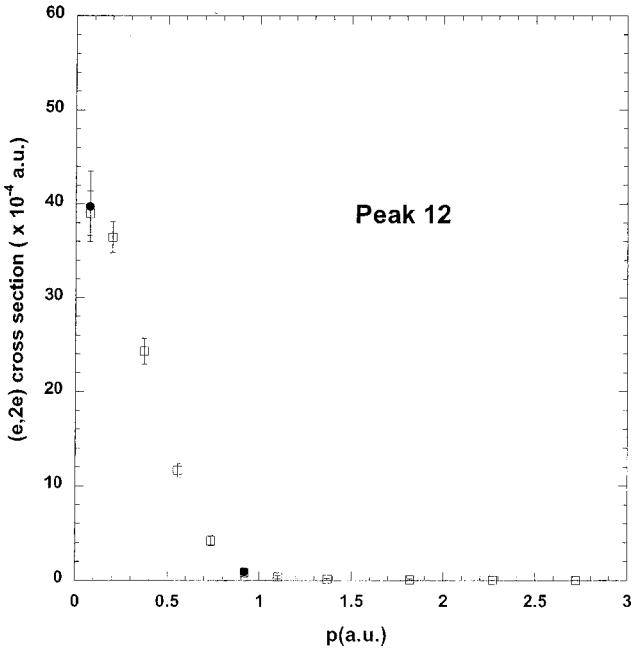

FIG. 9. 1500 eV symmetric noncoplanar MD for band 12 of the EMS binding energy spectra. The present data for run *A* (●) and run *B* (□) are shown.

ADC(3)/cc-pVDZ results (Table III) which suggest that up to 23.5%, 30.3%, and 27.5% of the $2a_1$, $1b_1$, and $1b_2$ fluxes might reside under peak 12, respectively, in the form of long correlation tails[52] consisting of shake-up lines with a spectroscopic strength smaller than 0.005. However, even upon admitting that this missing fraction of the $2a_1$ shake-up intensity would be entirely recovered under peak 12, it would still be far too small to explain the intensity of this peak in the spectrum recorded at the azimuthal angle $\phi=0°$, relative to that of band 11 [Fig. 1(a)]. This, the fact that the 1p-GF/ADC(3) and density functional theories of ionization and $(e,2e)$ cross sections provide very consistent insights into the shape, energy location, and into the momentum distributions characterizing the neighboring peaks 11 and 13, and the vast experience accumulated over the last 25 years with 1p-GF calculations of the shake-up transitions of saturated hydrocarbons[51–53] and many other molecules (see, for instance, Refs. 40, 42, 55–57 and references therein), lead us to believe that band 12 does not belong to the vertical one-electron and $2h$-$1p$ shake-up ionization spectrum of norbornane in its ground electronic state, as described by the ADC(3) model of ionization. A band-Lanczos study of the correlation tails in the ionization spectrum of NBA might be, however, useful to fully confirm this assertion.

Finally, we note that there are still quite a few orbital MD's that we have not specifically discussed or plotted in this section. Plots of these MD's are available on request to the corresponding author (M.J.B.). These MD's reinforce the argument for the utility of BP/TZVP that we have made in this section, but do not add any further insight.

VI. MOLECULAR PROPERTY INFORMATION

We now use the BP/TZVP model which best described the experimental MD's to derive the structure and a selection of the molecular properties of norbornane. These are compared in detail with independent experimentally determined values and those from other MO calculations, to determine how well the BP/TZVP model was able to reproduce these molecular properties.

A. Molecular geometries

In general, our calculations of molecular geometries using the BP/TZVP model are in very good agreement with experimentally determined molecular geometries (given the experimental uncertainties), and compare favorably with the results from other MO calculations. The results are summarized in Table IV. Note that in Table IV we have also included relevant data from our B3LYP/cc-pVTZ and MP2/aug-cc-pVDZ calculations. While these basis sets were not prevalidated using our EMS MD's, we have included them for completeness and in general their results appear to compare well with those from BP/TZVP. Further note that to assist the reader in the discussion that follows, a structural representation and atom numbering of the norbornane molecule is given in Fig. 10.

The two single bonds (C_2-C_3 and C_5-C_6) involving the four methylene carbon-carbon have bond distances of 1.571 Å from our calculations, in excellent agreement with the two experimental values of 1.573 Å from an electron diffraction study,[4,6] and 1.578 Å from Fitch and Jobic's powder x-ray diffraction study.[5] The remaining carbon-carbon bonds involving the bridge or bridgehead carbon atoms are also in excellent agreement with experiment. The agreement with experiment is better than for the small basis set *ab initio* and semiempirical MO-derived geometries in Table IV.[8,58] The distance between the two single bonds involving the four methylene carbon atoms (C_2-C_3 and C_5-C_6) was particularly well reproduced with the $C_2\cdots C_6$ distance from BP/TZVP of 2.520 Å compared with the experimental distance of 2.542 Å from powder x-ray diffraction studies.

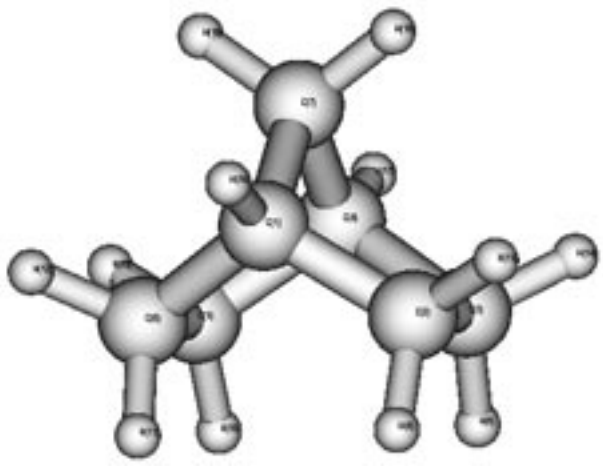

FIG. 10. Structural representation of norbornane and the atom numbering.

Bond angles were also well reproduced, especially the bridge and bridgehead angles. The bridge angle (e.g., $\angle C_1C_7C_4$) of 94.5° from our DFT calculations compares well with 93.1° from the x-ray structure and 93.4° from electron diffraction. The bridgehead angles (e.g., $\angle C_2C_1C_7$) were calculated to be 101.4° by our DFT calculation, compared with 102.0° from electron diffraction studies, and 99.3° from the x-ray diffraction studies. There was some evidence of lattice perturbations in the x-ray structure when compared with the electron diffraction structure and the structures predicted by MO methods, as illustrated in Table IV. For example, the bridgehead bond angle $\angle C_2C_1C_6$ is substantially larger in the x-ray structure than in the other experimental and theoretical structures, as is the angle $\angle C_1C_2C_3$, which is approximately 4° larger than in the other structures.

B. Dipole moment

Like all saturated hydrocarbons, norbornane has a small dipole moment which has been well reproduced by our BP/TZVP DFT calculations. We obtain a value of 0.076 D from our calculations compared with a very accurate value of 0.091(8) D inferred from the Stark effect in the microwave spectrum of norbornane.[3] Wilcox and co-workers had earlier estimated the dipole moment as 0.03(2) from dielectric measurements,[59] which appears to be too low.

TABLE V. ^{13}C NMR chemical shifts (in ppm).

Carbon	Experimental	BP/TZVP LORG	BP/TZVP IGLO	HF/6-31+G* GIAO (Ref. 66)	BP/TZVP GIAO[a]
1	36.8	46.5	47.8	33.2	43.0
2	30.1	35.0	36.3	27.4	34.6
3	30.1	35.0	36.3	27.4	34.6
7	38.7	43.5	45.2	34.4	41.9
6	30.1	35.0	36.3	27.4	34.6
5	30.1	35.0	36.3	27.4	34.6
4	36.8	46.5	47.8	33.2	43.0

[a]Results obtained using a B3LYP/6-31G* geometry.

C. NMR properties

There have been many measurements of the chemical shifts[60–62] of carbon and protons in norbornane, examples of which are the work of Abraham and co-workers[60] and Lippmaa *et al.*[61] We used the localized orbital/local origin (LORG),[63] individual gauge localized orbitals (IGLO) (Ref. 64) and gauge-independent atomic orbital (GIAO) methods[65] to calculate ^{13}C chemical shifts from our BP/TZVP calculations. Chemical shifts were determined by comparisons with the ^{1}H and ^{13}C isotropic shifts computed for tetramethylsilane at the BP/TZVP level. Our chemical shift values are compared in Tables V and VI with those determined by Sauers[66] from a GIAO calculation using Hartree–Fock theory. As in many previous computations of NMR chemical shifts (see Ref. 67 and references therein), these HF results systematically underestimate the experimental values whereas the opposite is seen with our BP/TZVP results.

The LORG method produced better agreement with the experimental ^{1}H and ^{13}C chemical shifts than the IGLO method, particularly for the proton spectrum. However, it appears that when a correlated wave function is used, the GIAO approach provides the best agreement with experiment. At this level, the chemical shifts for carbon predicted by our DFT calculations are overall in good agreement with the experimental shifts, although the bridgehead (methine) carbons had a larger error (~7 ppm) than the other (methylene) carbons (error ~3 ppm). The proton chemical shifts were in excellent agreement with experiment with an average error of 0.09 ppm. Put another way, at the GIAO level the BP/TZVP approach yields overestimates between 4% and 10%, in the experimental proton shifts.

The well-known differences in the chemical shifts between the *endo* and *exo* protons in norbornane are very nicely reproduced by our BP/TZVP calculations. At this level, and using the GIAO approach, we calculate a difference of 0.34 ppm compared with the experimental difference of 0.31 ppm.

TABLE VI. ^{1}H NMR chemical shifts (in ppm).

Proton	Experimental	BP/TZVP LORG	BP/TZVP IGLO	HF/6-31+G* GIAO (Ref. 66)	BP/TZVP GIAO[a]
1	2.19	2.36	4.56	1.91	2.28
2	1.16	1.27	3.32	1.12[b]	1.28
2′	1.47	1.49	3.68	1.37[b]	1.62
3	1.16	1.27	3.32	1.12[b]	1.28
3′	1.47	1.49	3.68	1.37[b]	1.62
4	2.19	2.36	4.56	1.92[b]	2.28
5	1.16	1.27	3.32	1.12[b]	1.28
5′	1.47	1.49	3.68	1.37[b]	1.62
6	1.16	1.27	3.32	1.12[b]	1.28
6′	1.47	1.49	3.68	1.37[b]	1.62
7	1.18	1.23	3.08	1.13	1.25

[a]Results obtained using a B3LYP/6-31G* geometry.
[b]This work.

D. Vibrational spectra

The DFT calculations were able to calculate the frequencies of the vibrational modes of norbornane with reasonable accuracy. Table VII shows the vibrational frequencies calculated at the BP/TZVP level in the present work. The calculated intensities of the transitions are also in reasonable agreement with the observed[68] experimental IR spectrum of norbornane, as Table VII also illustrates. The level of agreement between our (unscaled) BP/TZVP frequencies and experiment is similar to that of the work of Shaw *et al.*,[69] who studied the norbornane infrared spectrum using a *rescaled* HF/3-21G *ab initio* force field. The assignment of the norbornane vibrational modes follows from the work of Levin and Harris.[70] For completeness we note that according to the dipole selection rules for IR spectroscopy, transitions from the zero-point level to the excited vibrational levels belonging to the a_2 irreducible representation of the C_{2v} point group are forbidden by symmetry.[71] One of these transitions is nonetheless detected in the IR spectrum of norbornane, in the form of an extremely weak line at 542 cm^{-1}. This line must thus be described as a hot band.

VII. CONCLUSIONS

We have reported on the first comprehensive EMS study into the complete valence electronic structure of norbornane, in conjunction with DFT calculations of orbital MD's and 1p-GF [OVGF and ADC(3)] calculations of the one-electron and shake-up ionization spectrum. Excellent agreement is generally found between the experimental PES and EMS binding energies on the one hand and the 1p-GF results on the other hand. Where a comparison is possible, pole strengths calculated by our 1p-GF procedures, certainly for the outer valence orbitals, were found to be largely consistent with those determined from our EMS MD data. Strong final state configuration interaction effects are predicted in our ADC(3) calculation for the inner valence $2a_1$, $1b_2$, $1b_1$, and $1a_1$ orbitals, and this prediction is consistent with the very significant band broadening observed at binding energies beyond ~22 eV. A striking discrepancy between one-particle Green's function theory and experiment has been noted, however. It takes the form of a very intense band at ~25 eV in the EMS spectrum recorded at an azimuthal angle $\phi=0°$, which could not be reproduced by the large scale ADC(3) calculations presented in this work. According to the related momentum distribution, this band has apparently *s*-type symmetry. Further theoretical studies will be needed to establish whether it relates, for instance, to shake-up transitions to particularly diffuse bound states, to double ioniza-

TABLE VII. Infrared vibrational frequencies and intensities.

Symmetry label	Mode	BP/TZVP spectrum		Experimental spectrum [Levin and Harris (Ref. 70)]		
		TZVP (cm^{-1})	Intensity (km mol^{-1})	Frequency (cm^{-1})	Intensity	Assignment
a_2	7	164.82	0.0			
b_2	8	332.85	0.2	344	w	$\upsilon 26,\upsilon 39,\upsilon 51$
a_1	9	392.74	0.0	407	w	$\upsilon 15$
b_1	10	437.64	0.0	485	w	$\upsilon 35$
a_2	11	532.85	0.0	542	vw	$\upsilon 14$
a_1	12	738.32	0.8	755	s	$\upsilon 13,\upsilon 99$
b_2	13	744.02	0.1			
b_1	14	776.35	0.4	787	ms	$\upsilon 24,\upsilon 37$
a_1	15	797.49	0.0			
b_2	16	804.12	2.7	814	s	
a_1	17	857.80	1.4	874	s	$\upsilon 13$
b_1	18	873.00	1.3	889	s	$\upsilon 48$
a_1	19	908.14	1.6	925	s	$\upsilon 11$
a_2	20	926.69	0.0			
b_1	21	927.12	0.5	949	m	$\upsilon 36,\upsilon 47$
a_2	22	937.65	0.0			
b_2	23	937.94	0.6	958	w	$\upsilon 23$
a_1	24	973.06	0.1	990	w	$\upsilon 10$
b_1	25	1004.32	0.4	1031	m	$\upsilon 35,\upsilon 46$
b_2	26	1054.78	0.2	1069	w	$\upsilon 31$
b_1	27	1092.25	0.1	1091	w	$\upsilon 22$
a_2	28	1103.68	0.0	1103	w	$\upsilon 34$
a_1	29	1125.17	1.0	1120	m	$\upsilon 9$
b_2	30	1136.82	0.3	1140	m	$\upsilon 33$
b_1	31	1186.00	3.2	1160	w	
a_2	32	1195.51	0.0	1207	m	$\upsilon 8,\upsilon 45$
b_2	33	1225.65	1.2	1217	mw	$\upsilon 30$
a_1	34	1236.83	1.0	1242	w	$\upsilon 32$
b_2	35	1242.20	0.0	1259	mw	$\upsilon 7$
a_2	36	1253.65	0.0			
a_2	37	1276.66	0.0			
a_1	38	1293.44	1.8	1274	w	
b_2	39	1293.70	2.6	1301	m	$\upsilon 44$
b_1	40	1297.16	0.0	1317	m	$\upsilon 19$
a_2	41	1433.85	0.0	1400	w	$\upsilon 31$
a_1	42	1439.98	7.3			
b_2	43	1446.88	2.1	1442	m	$\upsilon 18$
b_1	44	1452.03	5.9	1455	s	$\upsilon 6,\upsilon 30,\upsilon 43$
a_1	45	1475.76	0.5	1465		$\upsilon 5$
b_2	46	2962.27	59.9			
a_2	47	2963.18	0.0			
a_1	48	2964.46	51.4			
b_1	49	2973.15	95.4			
a_1	50	2973.44	15.6			
a_2	51	2996.72	0.0			
b_2	52	2998.48	10.8			
b_1	53	3012.16	91.4	2866	m	
b_2	54	3012.82	4.2	2912	m	
a_1	55	3016.85	1.9	2928	m	
b_1	56	3017.78	62.8	2954	vs	
a_1	57	3022.19	94.0	2964	vs	

tion processes, or to autoionization via electronically excited and dissociating states.[72] The latter suggestion is in particular worthy of consideration, in light of the extent of the cyclic strains in a compound such as norbornane. On the experimental side, further He(II), Penning ionization and XPS studies of the innermost valence levels of norbornane are also clearly necessary.

Momentum distributions for the $3a_2+5b_2$, $7a_1$, $5b_1+6a_1$, $4b_2+2a_2+4b_1$, $3b_2+3b_1$, $5a_1+2b_1$, $4a_1$, $2b_2$, $3a_1$, $1a_2$, $2a_1+1b_2+1b_1$, and $1a_1$ orbitals were measured and compared against a series of PWIA-based calculations using DFT DGAUSS basis sets. Our calculations, for each of the three basis sets (DZVP, DZVP2, TZVP), were performed using both BP and BLYP exchange correlation corrections to the DFT functional. On the basis of this comparison between the experimental and theoretical MD's, we found that BP/

TZVP provided the most physically reasonable representation of the NBA wave function. Molecular property information derived from this ''optimum'' BP/TZVP wave function was seen to be in generally good agreement with the results from independent measurements. This provides compelling evidence for the pedigree of EMS in *a priori* evaluation of a quantum chemical wave function. For a molecule such as NBA, where unambiguous molecular geometry information is not readily available from traditional methods, this can be particularly useful.

Our next major study will concentrate on the valence electronic structure of norbornene (C_7H_{10}, NBN). We propose this investigation in order to probe how the electronic structure of the chemically similar nonbonnadione (C_7H_8, NBD, NBN, and NBA molecules changes as the double bonds of NBD are progressively saturated. That study will search for any discernible trends, particularly in the momentum distributions, and if so can we quantify them in a logical manner.

Finally, the present work highlights the need for implementing more efficient diagonalization approaches that preserve the total spectral moments for exhaustively studying with larger basis sets the innermost correlation tails in the 1p-GP/ADC(3) ionization spectra. Also, we note that an improvement in the $(e,2e)$ reaction mechanism description, particularly for the inner valence and core orbitals, by the development of a distorted wave framework[9] for multicentred targets (i.e., molecules) is still desirable. While this is a very difficult task, a clear need for its implementation exists.

ACKNOWLEDGMENTS

This work was supported in part by the Australian Research Council, and we thank Ms. Marilyn Mitchell for typing the manuscript. One of us (W.R.N.) acknowledges Flinders University for his visiting research fellowship, while another (K.L.N.) thanks the Ferry Trust for her scholarship. F.W. acknowledges the Australian Partnership for Advanced Computing (APAC) for use of their facilities. M.S.D., S.K., and J.P.F. acknowledge financial support from the Bijzonder Onderzoeks Fonds (BOF) of the Limburgs Universitair Centrum, and from the Fonds voor Wetenschappelijk Onderzoek_Vlaanderen (FWO) of the Flemish Branch of the National Scientific Foundation of Belgium. M.S.D. is indebted to Professor L. S. Cederbaum, University of Heidelberg, for useful discussions on Green's function theories.

[1] C.-Y. Zhao, Y. Zhang, and X.-Z. You, J. Phys. Chem. A **101**, 5174 (1997).
[2] Y. Morino, K. Kutchitsu, and A. Yokozeki, Bull. Chem. Soc. Jpn. **40**, 1552 (1967).
[3] A. Choplin, Chem. Phys. Lett. **71**, 503 (1980).
[4] J. F. Chiang, C. F. Wilcox, and S. H. Bauer, J. Am. Chem. Soc. **90**, 3149 (1968).
[5] A. N. Fitch and H. Jobic, J. Chem. Soc., Chem. Commun. **1993** 1516.
[6] L. Doms, L. van den Enden, H. J. Geise, and C. van Alsenoy, J. Am. Chem. Soc. **105**, 158 (1983).
[7] N. L. Allinger, H. J. Geise, W. Pyckhout, L. A. Paquette, and J. C. Gallucci, J. Am. Chem. Soc. **111**, 1106 (1989).
[8] J. Walkimar, J. W. Carneiro, P. R. Seidl, G. R. Tostes, and C. A. Taft, J. Mol. Struct.: THEOCHEM **152**, 281 (1987).
[9] E. Weigold and I. E. McCarthy, *Electron Momentum Spectroscopy* (Kluwer Academic/Plenum, New York, 1999).
[10] M. J. Brunger and W. Adcock, J. Chem. Soc., Perkin Trans. 2 **2002**, 1.
[11] P. Bischof, J. A. Hashmall, E. Heilbronner, and V. Harnung, Helv. Chim. Acta **52**, 1745 (1969).
[12] M. Getzlaff and G. Schönhense, J. Electron Spectrosc. Relat. Phenom. **95**, 225 (1998).
[13] G. Bieri, F. Burger, E. Heilbronner, and J. P. Maier, Helv. Chim. Acta **60**, 2213 (1977).
[14] N. Bodor, M. J. S. Dewar, and S. D. Worley, J. Am. Chem. Soc. **92**, 19 (1970).
[15] H. Mackenzie-Ross, M. J. Brunger, F. Wang, W. Adcock, N. Trout, I. E. McCarthy, and D. A. Winkler, J. Electron Spectrosc. Relat. Phenom. **123**, 389 (2002).
[16] H. Mackenzie-Ross, M. J. Brunger, F. Wang *et al.*, J. Phys. Chem. A **106**, 9573 (2002).
[17] F. Wang, M. J. Brunger, and D. A. Winkler, J. Phys. Chem. Solids (to be published).
[18] R. Bicker, H. Kessler, and G. Zimmermann, Chem. Ber. **111**, 3200 (1978).
[19] I. E. McCarthy and E. Weigold, Rep. Prog. Phys. **54**, 789 (1991).
[20] P. R. Bevington and D. K. Robinson, *Data Reduction and Error Analysis for the Physical Sciences* (McGraw-Hill, New York, 1990).
[21] I. E. McCarthy and E. Weigold, Rep. Prog. Phys. **51**, 299 (1988).
[22] M. Casida, Phys. Rev. A **51**, 2005 (1995).
[23] W. Kohn and L. J. Sham, Phys. Rev. **140**, A1133 (1965).
[24] A. D. Becke, Phys. Rev. A **38**, 3098 (1988).
[25] A. D. Becke, J. Chem. Phys. **88**, 2547 (1988).
[26] J. P. Perdew, Phys. Rev. B **33**, 8822 (1986).
[27] C. Lee, W. Yang, and R. G. Parr, Phys. Rev. B **37**, 785 (1988).
[28] J. Andzelm and E. Wimmer, J. Chem. Phys. **96**, 1280 (1992).
[29] A. Komornicki and G. J. Fitzgerald, J. Chem. Phys. **98**, 1398 (1993).
[30] M. T. Michalewicz, M. J. Brunger, I. E. McCarthy, and V. M. Norling, in *Proceedings of the CRAY Users Group*, edited by R. Shaginaw (1995), pp. 37–41.
[31] M. W. Schmidt, K. K. Baldridge, J. A. Boatz *et al.*, J. Comput. Chem. **14**, 1347 (1993).
[32] S. Hamel, P. Duffy, M. Casida, and D. R. Salahub, J. Electron Spectrosc. Relat. Phenom. **123**, 345 (2002).
[33] L. Frost and E. Weigold, J. Phys. B **15**, 2531 (1982).
[34] W. Adcock, M. J. Brunger, C. I. Clark, I. E. McCarthy, M. T. Michalewicz, W. von Niessen, E. Weigold, and D. A. Winkler, J. Am. Chem. Soc. **119**, 2896 (1997).
[35] W. Adcock, M. J. Brunger, I. E. McCarthy, M. T. Michalewicz, W. von Niessen, F. Wang, and E. Weigold, J. Am. Chem. Soc. **122**, 3892 (2000).
[36] N. Godbout, D. R. Salahub, J. Andzelm, and E. Wimmer, Can. J. Chem. **70**, 560 (1992).
[37] B. I. Dunlap, J. W. D. Conolly, and J. R. Sabin, J. Chem. Phys. **71**, 4993 (1979).
[38] A. D. Becke, J. Chem. Phys. **98**, 5648 (1993).
[39] J. Schirmer, L. S. Cederbaum, and O. Walter, Phys. Rev. A **28**, 1237 (1983).
[40] W. von Niessen, J. Schirmer, and L. S. Cederbaum, Comput. Phys. Rep. **1**, 57 (1984).
[41] J. Schirmer and G. Angonoa, J. Chem. Phys. **91**, 1754 (1989).
[42] H.-G. Weikert, H.-D. Meyer, L. S. Cederbaum, and F. Tarantelli, J. Chem. Phys. **104**, 7122 (1996).
[43] T. H. Dunning, Jr., J. Chem. Phys. **90**, 1007 (1989).
[44] M. S. Deleuze, Int. J. Quantum Chem. **93**, 191 (2003).
[45] F. Tarantelli, A. Sgamellotti, L. S. Cederbaum, and J. Schirmer, J. Chem. Phys. **86**, 2201 (1987).
[46] L. S. Cederbaum and W. Domcke, Adv. Chem. Phys. **36**, 205 (1977).
[47] V. G. Zakrewski and W. von Niessen, J. Comput. Chem. **14**, 13 (1993).
[48] M. J. Frisch, G. W. Trucks, H. B. Schlegel *et al.*, GAUSSIAN 98, Revision A.7, Gaussian Inc., Pittsburgh, MA, 1998; GAUSSIAN 03 (Gaussian Inc., Pittsburgh, MA, 2003).
[49] R. A. Kendall, T. H. Dunning, Jr., and R. J. Harrison, J. Chem. Phys. **96**, 6796 (1992).
[50] M. S. Deleuze, J. Delhalle, B. T. Pickup, and S. Svensson, J. Am. Chem. Soc. **116**, 10715 (1994).
[51] M. S. Deleuze and L. S. Cederbaum, J. Chem. Phys. **105**, 7583 (1996).
[52] A. Golod, M. S. Deleuze, and L. S. Cederbaum, J. Chem. Phys. **110**, 6014 (1999).
[53] M. S. Deleuze, W. N. Pang, A. Salam, and R. C. Shang, J. Am. Chem. Soc. **123**, 4049 (2001).
[54] Y. Zheng, W. N. Pan, R. C. Shang, X. J. Chen, C. E. Brion, T. K. Ghanty, and E. R. Davidson, J. Chem. Phys. **111**, 9526 (1999).

[55] M. S. Deleuze, J. Chem. Phys. **116**, 7012 (2002).
[56] L. S. Cederbaum, W. Domcke, J. Schirmer, and W. von Niessen, Adv. Chem. Phys. **65**, 115 (1986).
[57] M. S. Deleuze, A. B. Trofimov, and L. S. Cederbaum, J. Chem. Phys. **115**, 5859 (2001).
[58] C. R. Castro, R. Dutler, A. Rauk, and H. Wieser, J. Mol. Struct.: THEOCHEM **152**, 241 (1987).
[59] C. F. Wilcox, J. G. Zajacek, and M. F. Wilcox, J. Org. Chem. **30**, 2621 (1965).
[60] R. J. Abraham and J. Fisher, THEOCHEM **25**, 25 (1985).
[61] E. Lippmaa, A. A. Bobyleva, A. N. Kalinichenko, M. D. Ordubadi, and A. F. Platé, Org. Magn. Reson. **8**, 74 (1976).
[62] P. R. Seidl, K. Z. Leal, V. E. J. Costa, and N. D. Poli, Magn. Reson. Chem. **28**, 869 (1990).
[63] W. Kutzelnigg, Isr. J. Chem. **19**, 193 (1980).
[64] V. G. Malkin, O. L. Malkina, and D. R. Salahub, Chem. Phys. Lett. **204**, 80 (1993).
[65] K. Wolinski, J. F. Hinton, and P. Pulay, J. Am. Chem. Soc. **112**, 8251 (1990).
[66] R. R. Sauers, Tetrahedron **54**, 337 (1998).
[67] D. B. Chestnut, in *Reviews in Computational Chemistry*, edited by K. B. Lipkowitz and D. B. Boyd (VCH, New York, 1996), pp. 245–297.
[68] NIST Chemistry WebBook (see http://webbook.nist.gov/chemistry).
[69] R. A. Shaw, C. R. Castro, R. Dutler, A. Rauk, and H. Weiser, J. Chem. Phys. **89**, 716 (1988).
[70] I. W. Levin and W. C. Harris, Spectrochim. Acta, Part A **29**, 1815 (1973).
[71] G. Herzberg, *Infrared and Raman Spectra* (Van Nostrand Reinhold, New York, 1945).
[72] N. Kishimoto, E. Matsumura, K. Ohno, and M. S. Deleuze, J. Chem. Phys. **121**, 3074 (2004).